

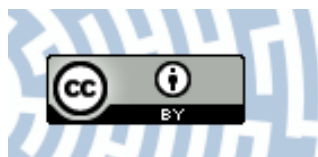


You have downloaded a document from
RE-BUŚ
repository of the University of Silesia in Katowice

Title: Symmetry of hR and Pseudo-hR Lattices

Author: Kazimierz Stróż

Citation style: Stróż Kazimierz. (2019). Symmetry of hR and Pseudo-hR Lattices. W: T. Akitsu (ed.), “Symmetry (Group Theory) and Mathematical Treatment in Chemistry” (S. 190-223). London : IntechOpen, doi 10.5772/intechopen.72314



Uznanie autorstwa - Licencja ta pozwala na kopowanie, zmienianie, rozpowszechnianie, przedstawianie i wykonywanie utworu jedynie pod warunkiem oznaczenia autorstwa.

Symmetry of *hR* and Pseudo-*hR* Lattices

Kazimierz Stróż

Additional information is available at the end of the chapter

<http://dx.doi.org/10.5772/intechopen.72314>

Abstract

Matrix methods for metric symmetry determination are fast, efficient, reliable, and, in contrast to reduction techniques, allow to establish simply all possible pseudo-symmetries in the vicinity of higher symmetry borders. It is shown that distances to borders may be characterized by one or a few monoaxial deformations measured by parameter ε , which corresponds to the relative change in the interplanar distance. The scope of this chapter is limited to a careful analysis of rhombohedral or monoclinic deformations occurring in *hR* lattices.

Keywords: semi-reduced lattices, lattice symmetry, Bravais type border, lattice deformation

1. Introduction

Chemical species are structurally classified by symmetry. The preliminary classification takes into account only translational properties, the *lattice* of a crystal structure. But identical lattices may be described by an infinite number of different unit cells ($a, b, c, \alpha, \beta, \gamma$ or corresponding metric tensor G) and thus it is important to select finally the reference cell called the *Bravais cell*, which symmetry reflects the lattice symmetry. While the derivation of unit cell parameters from good X-ray diffraction data is generally straightforward, the problem of symmetry-standardization is challenging [1], especially in the presence of random errors, pseudo-symmetry caused by the vicinity of Bravais type boundaries, textures, etc. Stable algorithms should recognize admissible symmetry and pseudo-symmetry(-tries) and calculate the distance(s) from the experimental unit-cell data to the Bravais lattice(s) subspace. Conceptually, a similar problem arises in the determination of distances between pairs of unit cells for database searching. A concise review of commonly used lengths (metrics) and its application to protein database search [2] showed that there is still room for improvements to characterize better the lattice on the symmetry borders. Advances in X-ray

diffraction techniques as well as improvements in data analyzing procedures allow to conclude that some of the previously obtained results may be based on pseudo-symmetry rather than on true symmetry (typical dilemma: hR or mC ?). Some new diffraction data suggest, for example, that generally accepted trigonal crystal structures $\alpha\text{-Cr}_2\text{O}_3$, $\alpha\text{-Fe}_2\text{O}_3$, and CaCO_3 show monoclinic distortions [3, 4]. In consequence, the importance of border problems has a growing-up tendency.

Classifications of unique lattice representatives obtained by the *Niggli reduction* or *Delaunay reduction* are commonly used techniques to assign the Bravais symmetry to a given lattice. Another approach, called the *matrix method*, directly derives isometric transformations from the lattices by B -matrices, which transform a lattice onto itself [1, 5, 6], or by the space distribution of orthogonalities [7], or by filtering predefined set V of 480 potential symmetry matrices [8, 9]. The latter technique is applicable to a wide class of semi-reduced lattice descriptions, additionally forced by a geometric interpretation of symmetry operations. The following advantages seem to be apparent: (i) the filtering process is extremely simple, (ii) semi-reduced lattices after a small deformation are generally still semi-reduced, (iii) symmetry axes and planes are automatically indexed, (iv) a lattice deformation, which retains the given symmetry, is easily deduced. The property (iv) can be utilized as a ‘distortion index’, a new measure of the distance between symmetrical lattices. The aim of this chapter is to carefully look at the border problems frequently occurring in hR lattices ($hR\text{-}cF$, $hR\text{-}cP$, $hR\text{-}cI$, $hR\text{-}mC$), but in the less-known *semi-reduced* lattice representations. Two appended real-life examples explain deeper the proposed technique and its possibilities.

2. Semi-reduced lattice descriptions

The concept of a semi-reduced lattice description (s.r.d.) has been given elsewhere [9]. The emphasis on the crystallographic features of lattices was obtained by shifting the focus (i) from the analysis of a lattice metric to the analysis of symmetry matrices [6], (ii) from the geometric interpretation of isometric transformation based on invariant subspaces to the orthogonality concept [7] extended to splitting indices [8], (iii) and from predefined cell transformations to transformations derivable via geometric information [6, 7]. It was shown that both corresponding arithmetic and geometric holohedries share the space distribution of symmetry elements and thus simplify the crystallographic description of structural phase transitions, especially those observed with the use of powder diffraction. Moreover, the completeness of s.r.d. types revealed a combinatorial structure of V (see below).

The main result of introduced semi-reduced lattice representations consists in the extension of the famous characterization of Bravais lattices according to their metrical, algebraic, and geometric properties onto a wide class of primitive, less restrictive lattices (including Niggli-reduced, Buerger-reduced, nearly Buerger-reduced, and a substantial part of Delaunay-reduced). While the *geometric* operations in Bravais lattices map the basis vectors onto themselves, the *arithmetic* operators in s.r.d. transform the basis vectors into cell vectors (basis vectors, face or space diagonals) and are represented by matrices from the set V of 480 matrices with the determinant 1 and elements $\{0, \pm 1\}$ of the matrix powers. A lattice is in s.r.d. if the

absolute values of off-diagonal elements in both metric tensors G and G^{-1} are smaller than the corresponding two diagonal elements sharing the same column and sharing the same row. The experimental s.r.d. metric G must be unchanged (with some relaxation) by the symmetry operation from V , thus by simple filtering:

$$G' = V^T G V, V \in V \text{ and } (a, b, c, \alpha, \beta, \gamma) \rightarrow G \sim G' \rightarrow (a', b', c', \alpha', \beta', \gamma') \quad (1)$$

and the subsequent geometric interpretation of the filtered matrices leads to mathematically stable and rich information on the individual transformation bringing the lattice into coincidence with itself (known as an *isometry* or a *symmetry operation*) and deviations from the exact match:

$$\Delta a/a\%, \Delta b/b\%, \Delta c/c\%, \Delta \alpha^\circ, \Delta \beta^\circ, \Delta \gamma^\circ, \delta^\circ, \quad (2)$$

where $\Delta a/a\%$ denotes $(a' - a)/a \cdot 100[\%]$, $\Delta \alpha^\circ = \alpha' - \alpha^\circ$ and δ° is Le Page parameter [7]. For exact isometric transformation, all such discrepancy parameters should be zero (or very close to zero).

It is obvious that symmetry operations fulfill the closure, associative, identity, and inverse axioms and form a group: an *arithmetic holohedry* or in other words a *lattice group*. The set V of all possible transformations in s.r.d. is covered by the arithmetic holohedries of 39 highest symmetry lattices (**Table 1**).

In the s.r.d. approach, the primitive-to-Bravais transformations are not stored, but dynamically constructed, based on the geometric interpretation of symmetry matrices. Unfortunately, the classical symbol of a point or space symmetry operation bears information on an operation type and a 1D subspace (or 2D in the case of symmetry planes) of points invariant under this operation [10], but the information on the complement orthogonal subspace, invariant as a whole, is lost. In the developed *splitting* or *dual* symbol introduced in [8], orientation of

Lattice	Metric	Lattice	Metric	Lattice	Metric	Lattice	Metric
hP_1	2,2,1,0,0,-1	hP_4	2,2,1,0,0,1	cF_7	2,2,2,0,-1,-1	cI_7	4,3,3,1,2,2
hP_2	2,1,2,0,-1,0	hP_5	2,1,2,0,1,0	cF_8	2,2,2,1,1,0	cI_8	3,3,4,-2,-2,1
hP_3	1,2,2,-1,0,0	hP_6	1,2,2,1,0,0	cF_9	2,2,2,1,0,1	cI_9	3,4,3,-2,1,-2
cP_0	1,1,1,0,0,0			cF_{10}	2,2,2,0,1,1	cI_{10}	4,3,3,1,-2,-2
cF_1	2,2,2,1,1,1	cI_1	3,3,3,-1,-1,-1	cF_{11}	2,2,2,1,-1,0	cI_{11}	3,3,4,-2,2,-1
cF_2	2,2,2,-1,-1,1	cI_2	3,3,3,1,1,-1	cF_{12}	2,2,2,1,0,-1	cI_{12}	3,4,3,-2,-1,2
cF_3	2,2,2,-1,1,-1	cI_3	3,3,3,1,-1,1	cF_{13}	2,2,2,0,1,-1	cI_{13}	4,3,3,-1,-2,2
cF_4	2,2,2,1,-1,-1	cI_4	3,3,3,-1,1,1	cF_{14}	2,2,2,-1,1,0	cI_{14}	3,3,4,2,-2,-1
cF_5	2,2,2,-1,-1,0	cI_5	3,3,4,2,2,1	cF_{15}	2,2,2,-1,0,1	cI_{15}	3,4,3,2,-1,-2
cF_6	2,2,2,-1,0,-1	cI_6	3,4,3,2,1,2	cF_{16}	2,2,2,0,-1,1	cI_{16}	4,3,3,-1,2,-2

Metrics corresponding to lattice descriptions $cI_5 - cI_{16}$ determine non-Buerger cells.

Table 1. Complete set M of metrical tensors of highest-symmetry lattices referred to semi-reduced bases [8].

both subspaces is given by specifying direction $[uvw]$ orthogonal to the family of planes (hkl) . The centering in the $[uvw]$ direction as well as the crystallographic orthogonality between a lattice direction and a lattice plane, hidden in the symmetry matrix, is enclosed in this new geometric symbol $n^{(+/-)}[uvw](hkl)$. Some properties of $[uvw](hkl)$ are mathematically obvious; splitting indices specify the same vector, or more strictly, a pair of parallel directions in direct and reciprocal spaces. Others, like calculations of the interplanar distance $d_{(hkl)}$, the distance between lattice points $l_{[uvw]}$, deriving Le Page angle δ [7] between $[uvw]$ and (hkl) , or even using indices to predict deformations, which retain a given cyclic group, need additionally G data. In a lattice given by G , the uniaxial deformation along symmetry $[uvw]$ direction

$$G' = G + \varepsilon \begin{pmatrix} hh & hk & hl \\ kh & kk & kl \\ lh & lk & ll \end{pmatrix} \quad (3)$$

modifies only 1D subspace and in consequence retains the symmetry axis in $[uvw]$ direction and also axes orthogonal to this direction, if any. Other symmetries will be broken.

3. Rhombohedral lattices in s.r.d.

It is difficult to classify or compare lattices that drastically change their class-dependent descriptions as a result of small deformations, structural phase transitions, or experimental errors. Such discontinuities in the Niggli-reduced space can be overcome by a deep mathematical treatment like in [11] or by applying a less restrictive method of Bravais cell assignment: Niggli reduction \rightarrow Delaunay reduction \rightarrow s.r.d. A wide class of lattices, including a trigonal and three cubic lattices, is considered here as 'rhombohedral' lattices. The actual form of a cell has no meaning, but a given lattice can be represented by a rhombohedron with equal sides $a = b = c$ and angles $\alpha = \beta = \gamma$. The symmetry does not depend on the scale, so we can assume that all sides are equal to 1 and thus the class is one-parametric with the rhombohedral angle α , $0^\circ < \alpha < 120^\circ$. Symmetry matrices of 'rhombohedral' lattices cover V nearly completely (excluding 6 hexagonal groups). As mentioned earlier, every symmetry matrix describes an isometric transformation of basis vectors into cell vectors. Neglecting the vector sense, there are 13 cell vectors grouped in the rhombohedral case into four triads $<001>, <011>, <01-1>, <1-1-1>$ of directions related by three-fold axis along $[111]$. Triad $<01-1>$ corresponds to twofold axes. Moreover, lattice vector $[111]$ is orthogonal to coplanar vectors $<01-1>$, which interaxial angle is 60° . Thus, symmetry matrices of hR lattice in the Bravais description ($a = b = c, \alpha = \beta = \gamma < 120^\circ$) are characterized by dual symbols: $3^+111, 3^-111, 201-1, 21-10, 2-101$ and this geometric property is exposed in the hexagonal description with $c/a = l_{[111]}/l_{<01-1>}$. Metrical relationships between lengths of cell vectors as functions of α are drawn in **Figure 1**.

The angle $\alpha = 90^\circ$ and a cubic shape can be considered as the central point of the sketch. Both left and right parts separated by 90° are connected by the lattice inversion. Other characteristic points (i.e., intersection of curves) are collected in **Table 2**.

Information contained in both **Figure 1** and **Table 2** explains discontinuities in descriptions of rhombohedral lattices. Descriptions of Niggli- or Buerger-reduced lattices must be changed during crossing characteristic angles 60° and 109.47° , since they are based on the shortest

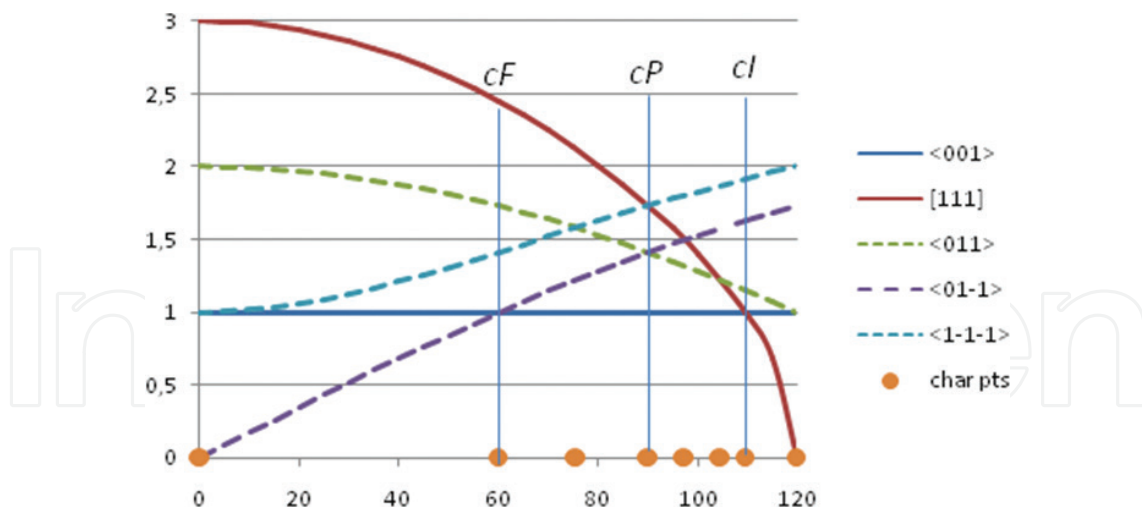


Figure 1. Lengths of cell vectors as a function of rhombohedral angle. Intersections of curves define characteristic points (e.g., higher symmetry lattices: *cF*, *cP*, and *cl*).

No.	$\cos(\alpha)$	$\alpha[^\circ]$	Description
1	1	0	1D
2	1/2	60	<i>cF</i>
3	1/4	75.5225	$c/a = \sqrt{3}$
4	0	90	<i>cP</i>
5	-1/8	97.1808	$c/a = \sqrt{3/3}$
6	-1/4	104.4775	$c/a = \sqrt{3/5}$
7	-1/3	109.4712	<i>cl</i>
8	-1/2	120	2D

Lattice *cP* (point 4) maximally extended along [111] reduces 3D space to the 1D (point 1); maximal compression leads to 2D space (point 8). Intermediate points (2, 7) correspond to centered lattices: *cF*, *cl*. Other intersections (points 5 and 6) have no influence on symmetry.

Table 2. Characteristic points (intersections of curves) in Figure 1.

non-coplanar lattice vectors. Similarly, Bravais descriptions should reflect the increased symmetry for these angles (directions $<001>$ reveal extra twofold and threefold symmetry). In sharp contrast to the above lattice representations, no drastic changes are necessary in semi-reduced descriptions of rhombohedral lattices, without losing relation with Bravais standardization.

4. Distance to the higher symmetry border: ε concept

In crystallography, it is crucial to standardize lattice descriptions and to assign one from the fourteen 3D Bravais types differentiated by symmetry. The process is straightforward for good quality data and faraway from the Bravais borders but in opposite cases, especially in

the presence of unavoidable experimental errors, the solution cannot be unique. Usable distances should be defined to rank positive candidates. Most considerations about the calculation of such distances are devoted to the Niggli reduction, for example, see [11] and references contained therein; only some discuss the Buerger reduction [1, 7].

The geometric properties of matrices that transform an s.r.d. lattice into itself are utilized in the presented approach to the greatest degree, which form the *geometric image* of the filtered transformation. Each isometric or pseudo-isometric action on the current lattice is estimated by three metrical and four angular parameters (2) and oriented in the lattice space by dual indices $[uvw]$ ((hkl)). Deviations are controlled by two thresholds: metrical $tol1$ and angular $tol2$. The $maxdev$ (that is maximal value of all unsigned deviations for all isometric transformations grouped in the lattice symmetry) was selected as an introductory concept of similarity between the probe cell and a cell with given symmetry. For exact symmetry, $maxdev$ should be zero (or very close to zero). In the vicinity of symmetry borders, high values of $tol1$ and $tol2$ (e.g., 5) reveal higher pseudo- (in another words ‘approximate’) symmetry—with greater $maxdev$ values and standard group-subgroup relations (**Table 3**). For reasonable thresholds, the number of filtered matrices cannot exceed 24.

The filtering of symmetry matrices near cubic borders results in a rather big number (7×24) of quantitative data. As **Table 3** shows, deviations are interrelated, not random. A maximal unsigned deviation well reflects this situation. Moreover, strict hR symmetry including 2 isometries denoted geometrically as $3^{+(-)}[-1-13](001)$ and pseudo- cF symmetry suggest that all deviations can be explained by a rhombohedral deformation. According to (3), the uniaxial deformation along direction $[-1-13]$ orthogonal to planes (001) modifies metric G :

$$G' = \begin{pmatrix} 2 & 1 & 1 \\ 1 & 2 & 1 \\ 1 & 1 & 2.1 \end{pmatrix} + \varepsilon \begin{pmatrix} 0 & 0 & 0 \\ 0 & 0 & 0 \\ 0 & 0 & 1 \end{pmatrix}.$$

It is clear from **Table 1** that G' with cF symmetry should be $cF_1 = (2, 2, 2, 1, 1, 1)$. The above symmetric matrix equation can be rewritten in a vector form:

$$(2, 2, 2, 1, 1, 1) = (2, 2, 2.1, 1, 1, 1) + \varepsilon(0, 0, 1, 0, 0, 0)$$

with the solution $\varepsilon = -0.1$. As a result, distance ε between hR and cF cells is -0.1 . This new concept is more informative in comparison with $maxdev$ parameter; the deformation type is explicitly given by $\varepsilon \cdot (hkl)$ and can be converted into $\Delta d_{(hkl)} / d_{(hkl)}$, shortly $\Delta d/d$, and related with diffraction line shifts in XRD patterns. The ε distances depend not only on a rhombohedral angle but also on the lattice scale, and thus for practical purposes, the $\Delta d/d$ distance is more appropriate, since it can be compared with experimental $\Delta d/d$ resolution. The interplanar distance may be calculated from the following formula:

$$d_{(hkl)} = 1 / [(hkl) \cdot G \cdot (hkl)^T]^{1/2} \quad (4)$$

The sign of ε or Δd is also important; it informs on which side of the higher symmetry border the analyzed lattice is located.

For rhombohedral lattices, two kinds of ε distances to the border (based on rhombohedral or monoclinic deformations) are generally analyzed. In more complicated cases, like cubic lattices

$\Delta a/a\%$	$\Delta b/b\%$	$\Delta c/c\%$	$\Delta \alpha^\circ$	$\Delta \beta^\circ$	$\Delta \gamma^\circ$	δ°	Operation
0.00	0.00	0.00	0.00	0.00	0.00	0.00	1[]()
0.00	0.00	0.00	0.00	0.00	0.00	0.00	2[010](121)
0.00	0.00	0.00	0.00	0.00	0.00	0.00	21-10
0.00	0.00	0.00	0.00	0.00	0.00	0.00	2[100](211)
0.00	0.00	0.00	0.00	0.00	0.00	0.00	3 + [-1-13](001)
0.00	0.00	0.00	0.00	0.00	0.00	0.00	3-[-1-13](001)
0.00	2.47	-2.41	0.00	-0.79	0.79	1.95	201-1
2.47	2.47	0.00	-2.38	-2.38	-1.59	1.95	2[001](112)
2.47	0.00	-2.41	-0.79	0.00	0.79	1.95	2[-101](-1-1)
0.00	2.47	-2.41	0.00	-0.79	0.79	1.95	2[-111](011)
2.47	0.00	-2.41	-0.79	0.00	0.79	1.95	2[1-11](101)
2.47	2.47	0.00	-2.38	-2.38	-1.59	1.95	2[11-1](110)
0.00	2.47	-2.41	0.00	-0.79	0.79	1.30	3 + 111
2.47	0.00	-2.41	-0.79	0.00	0.79	1.30	3-111
0.00	2.47	-2.41	0.00	-0.79	0.79	1.30	3+ [3-1-1](100)
2.47	2.47	0.00	-2.38	-2.38	-1.59	1.30	3-[3-1-1](100)
2.47	2.47	0.00	-2.38	-2.38	-1.59	1.30	3 + [-13-1](010)
2.47	0.00	-2.41	-0.79	0.00	0.79	1.30	3-[-13-1](010)
2.47	0.00	-2.41	-0.79	0.00	0.79	1.95	4 + [-111](011)
2.47	2.47	0.00	-2.38	-2.38	-1.59	1.95	4-[-111](011)
2.47	2.47	0.00	-2.38	-2.38	-1.59	1.95	4 + (1-11)(101)
0.00	2.47	-2.41	0.00	-0.79	0.79	1.95	4-[1-11](101)
2.47	0.00	-2.41	-0.79	0.00	0.79	1.95	4+ [11-1](110)
0.00	2.47	-2.41	0.00	-0.79	0.79	1.95	4-[11-1](110)

Items with zero deviations define true *hR* symmetry ($a,b,c = 1.41421$, $\alpha,\beta,\gamma = 60.7941^\circ$) with $maxdev = 0$, while all 24 operations correspond to pseudo-*cF* symmetry ($a,b,c = 2.025$, $\alpha,\beta,\gamma = 91.3976^\circ$) with $maxdev = 2.47$.

Table 3. Geometric images (7 discrepancy parameters + geometric description) of filtered matrices for the lattice $G = (2, 2, 2.1, 1, 1, 1)$ and illustration of $maxdev$ distances.

modified by simultaneous rhombohedral and tetragonal distortions, few ϵ distances can be derived. Calculations are also possible in the presence of experimental errors, if they are smaller than distortions.

The concept of a quantitative measure between the probe cell and cells with higher symmetry based on monoaxial deformations is thus outlined, but for practical applications this idea should be thoroughly investigated in s.r.d. This study provides analyses and two real-life examples limited to rhombohedral lattices.

5. Distances between hR and cubic lattices

In the case being considered, the semi-reduced hR lattice should be viewed as a rhombohedrally distorted cF , cI , or cP pseudo-lattice with exact hR symmetry. It is also assumed that every equivalent description is equally distanced from a cubic lattice, and thus only one representation of a lattice is necessary to properly derive such distance. This assumption validity may be carefully checked by creating all semi-reduced variants of hR lattices in the neighborhood of cubic lattices.

5.1. hR - cF border

Let us have hR lattice in a standard description ($a,b,c = 1,449,138$; $\alpha,\beta,\gamma = 58,41,186^\circ$). It is obviously relatively close to cF lattice. The analysis of pseudo-symmetry outlined in Section 4 reveals that the distance ε to the higher symmetry is equal to -0.1 . An opposite deformation of 16 cF descriptions in **Table 1** according to 4 threefold axes allows to generate all 64 semi-reduced hR variants of the given lattice and thus relations in **Table 4** ' hR metric' + 'deformation' = cF are obvious. But, as verified by computer tests, the same deformations can be extracted also from the geometric images of pseudo-symmetry without any relation to the predefined cF metrics.

The interpretation of 4×16 items in **Table 4** is very easy due to the fact that Miller indices of planes perpendicular to the unique threefold axis are given explicitly in the deformation symbols. In the considered situation, the operation on G vectors is as follows: $G_{cF} = G_{hR} - 0.1 \cdot (hh, kk, ll, kl, hl, hk)$. For example, the last three items give:

$$(2, 1, 2, 2.1, 0, -1.1, 1) - 0.1 \cdot (-1\cdot-1, 0\cdot0, 1\cdot1, 1\cdot0, 1\cdot-1, -1\cdot0) = (2, 2, 2, 0, -1, 1)$$

$$(2, 2.1, 2, 0, -1, 1) - 0.1 \cdot (0\cdot0, 1\cdot1, 0\cdot0, 0\cdot1, 0\cdot0, 0\cdot1) = (2, 2, 2, 0, -1, 1)$$

$$(2, 2, 2.1, 0, -1, 1) - 0.1 \cdot (0\cdot0, 0\cdot0, 1\cdot1, 1\cdot0, 1\cdot0, 0\cdot1) = (2, 2, 2, 0, -1, 1)$$

Assigning the symmetry group to the final G metric or comparing it with **Table 1** reveals cF symmetry in cF_{16} description. In consequence, distance ε from $hR(a,b,c = 1.449138; \alpha,\beta,\gamma = 58.41186^\circ)$ to $cF(a,b,c = 2; \alpha,\beta,\gamma = 90^\circ)$ is equal to -0.1 and does not depend on the actual description. The original d spacing along threefold axis is changed from 1.1972 (hR lattice) to 1.1577 (cF lattice) and $\Delta d/d = -0.0355$. Such values characterize not only each item in **Table 4** but also all hR lattices with rhombohedral angle 58.41186°. Since ε corresponds with the rational part of G components in **Table 4**, similar tables of equivalent descriptions of hR (other ε) can be simply constructed. For example, the modification of rational parts from 0.1 to -0.01 will result in obtaining new hR lattice ($a,b,c = 1.410674; \alpha,\beta,\gamma = 60.1661^\circ$) with a shorter ε distance to cF border equal to 0.01.

5.2. hR - cI border

The hR lattice close to cI border seems to be less populated. The metrical relationships between the length of cell vectors look more complicated in comparison with cF neighborhood (**Figure 1**), but the analysis of pseudo-symmetries is similar. The same distance $\varepsilon = -0.1$ gives hR lattice with the rhombohedral angle 106.8773°. All semi-reduced descriptions together with deformations needed in order to obtain higher cI symmetry are compiled in **Table 5**.

hR metric						deformation	hR metric						deformation
2.1	2.1	2.1	1.1	1.1	1.1	-0.1·(111)	2.1	2.1	2	1	0	1.1	-0.1·(110)
2	2	2.1	1	1	1	-0.1·(001)	2	2.1	2.1	1.1	0	1	-0.1·(011)
2	2.1	2	1	1	1	-0.1·(010)	2	2	2.1	1	0	1	-0.1·(001)
2.1	2	2	1	1	1	-0.1·(100)	2.1	2	2	1	0	1	-0.1·(100)
2.1	2.1	2.1	-1	-1	1.1	-0.1·(-1-11)	2.1	2.1	2	0	1	1.1	-0.1·(110)
2	2	2.1	-1	-1	1	-0.1·(001)	2.1	2	2.1	0	1.1	1	-0.1·(101)
2	2.1	2	-1	-1	1	-0.1·(010)	2	2.1	2	0	1	1	-0.1·(010)
2.1	2	2	-1	-1	1	-0.1·(100)	2	2	2.1	0	1	1	-0.1·(001)
2.1	2.1	2.1	-1	1.1	-1	-0.1·(1-1 - 1)	2	2.1	2.1	1.1	-1	0	-0.1·(011)
2	2	2.1	-1	1	-1	-0.1·(001)	2.1	2	2.1	1	-1.1	0	-0.1·(-101)
2	2.1	2	-1	1	-1	-0.1·(010)	2	2.1	2	1	-1	0	-0.1·(010)
2.1	2	2	-1	1	-1	-0.1·(100)	2.1	2	2	1	-1	0	-0.1·(100)
2.1	2.1	2.1	1.1	-1	-1	-0.1·(-11-1)	2	2.1	2.1	1.1	0	-1	-0.1·(011)
2	2	2.1	1	-1	-1	-0.1·(001)	2.1	2.1	2	1	0	-1.1	-0.1·(1-10)
2	2.1	2	1	-1	-1	-0.1·(100)	2.1	2	2	1	0	-1	-0.1·(100)
2.1	2	2	1	-1	-1	-0.1·(010)	2	2	2.1	1	0	-1	-0.1·(001)
2	2.1	2.1	-1	-1	0	-0.1·(01-1)	2.1	2	2.1	0	1.1	-1	-0.1·(101)
2.1	2	2.1	-1	-1	0	-0.1·(-101)	2.1	2.1	2	0	1	-1.1	-0.1·(1-10)
2	2.1	2	-1	-1	0	-0.1·(010)	2	2.1	2	0	1	-1	-0.1·(010)
2.1	2	2	-1	-1	0	-0.1·(-101)	2.1	2.1	2	0	1	-1.1	-0.1·(1-10)
2	2.1	2	-1	-1	0	-0.1·(010)	2	2.1	2	0	1	-1	-0.1·(010)
2.1	2	2	-1	-1	0	-0.1·(100)	2	2	2.1	0	1	-1	-0.1·(001)
2	2.1	2.1	-1	0	-1	-0.1·(01-1)	2.1	2	2.1	-1	1.1	0	-0.1·(101)
2.1	2.1	2	-1	0	-1	-0.1·(1-10)	2	2.1	2.1	-1.1	1	0	-0.1·(01-1)
2.1	2	2	-1	0	-1	-0.1·(001)	2	2.1	2	-1	1	0	-0.1·(010)
2	2	2.1	-1	0	-1	-0.1·(100)	2.1	2	2	-1	1	0	-0.1·(100)
2.1	2.1	2	0	-1	-1	-0.1·(1-10)	2.1	2.1	2	-1	0	1.1	-0.1·(110)
2.1	2	2.1	0	-1	-1	-0.1·(-101)	2	2.1	2.1	-1.1	0	1	-0.1·(01-1)
2	2.1	2	0	-1	-1	-0.1·(010)	2.1	2	2	-1	0	1	-0.1·(100)
2	2	2.1	0	-1	-1	-0.1·(001)	2	2	2.1	-1	0	1	-0.1·(001)
2	2.1	2.1	1.1	1	0	-0.1·(011)	2.1	2.1	2	0	-1	1.1	-0.1·(110)
2.1	2	2.1	1	1.1	0	-0.1·(101)	2.1	2	2.1	0	-1.1	1	-0.1·(-101)
2.1	2	2	1	1	0	-0.1·(100)	2	2.1	2	0	-1	1	-0.1·(010)
2	2.1	2	1	1	0	-0.1·(010)	2	2	2.1	0	-1	1	-0.1·(001)

The illustration of hR lattice is represented by semi-reduced descriptions. Every four descriptions are close to one of the cF lattice variants given in **Table 1**, what is easily seen by rejecting a rational part in metric elements. The distance to the border $hR - cF$ is -0.1 , or -0.035514356 given in $\Delta d/d$ units, where d is an interplanar distance between a family of planes perpendicular to the threefold axis.

Table 4. Sixty-four semi-reduced descriptions of the same hR lattice ($a,b,c = 1,449,138$; $\alpha,\beta,\gamma = 58,41,186^\circ$) and its rhombohedral deformations to the cF lattice ($a,b,c = 2$; $\alpha,\beta,\gamma = 90^\circ$).

hR metric						deformation		hR metric						deformation	
3.1	3.1	3.1	-1	-1	-1	-0.1·(111)		3.1	4.4	3.9	-2.6	1.3	-2.2	-0.1·(1-23)	
3.1	3.9	3.1	-1	-1	-1	-0.1·(-13-1)		3.1	4.4	3.1	-1.8	0.9	-2.2	-0.1·(-121)	
3.1	3.1	3.9	-1	-1	-1	-0.1·(-1-13)		3.1	4.4	3.1	-2.2	0.9	-1.8	-0.1·(12-1)	
3.9	3.1	3.1	-1	-1	-1	-0.1·(3-1-1)		3.9	4.4	3.1	-2.2	1.3	-2.6	-0.1·(3-21)	
3.1	3.1	3.1	0.9	0.9	-1	-0.1·(-1-11)		4.4	3.9	3.1	1.3	-2.2	-2.6	-0.1·(-231)	
3.1	3.1	3.9	1.3	1.3	-1	-0.1·(113)		4.4	3.1	3.9	1.3	-2.6	-2.2	-0.1·(-213)	
3.1	3.9	3.1	1.3	0.9	-1	-0.1·(-131)		4.4	3.1	3.1	0.9	-2.2	-1.8	-0.1·(21-1)	
3.9	3.1	3.1	0.9	1.3	-1	-0.1·(3-11)		4.4	3.1	3.1	0.9	-1.8	-2.2	-0.1·(2-11)	
3.1	3.1	3.1	0.9	-1	0.9	-0.1·(-11-1)		3.1	3.1	4.4	-1.8	2.2	-0.9	-0.1·(112)	
3.1	3.1	3.9	1.3	-1	0.9	-0.1·(-113)		3.1	3.1	4.4	-2.2	1.8	-0.9	-0.1·(-1-12)	
3.1	3.9	3.1	1.3	-1	1.3	-0.1·(131)		3.1	3.9	4.4	-2.6	2.2	-1.3	-0.1·(-13-2)	
3.9	3.1	3.1	0.9	-1	1.3	-0.1·(31-1)		3.9	3.1	4.4	-2.2	2.6	-1.3	-0.1·(3-12)	
3.1	3.1	3.1	-1	0.9	0.9	-0.1·(1-1-1)		3.1	4.4	3.9	-2.6	-1.3	2.2	-0.1·(-1-23)	
3.1	3.1	3.9	-1	1.3	0.9	-0.1·(1-13)		3.1	4.4	3.1	-1.8	-0.9	2.2	-0.1·(121)	
3.1	3.9	3.1	-1	0.9	1.3	-0.1·(13-1)		3.1	4.4	3.1	-2.2	-0.9	1.8	-0.1·(1-21)	
3.9	3.1	3.1	-1	1.3	1.3	-0.1·(311)		3.9	4.4	3.1	-2.2	-1.3	2.6	-0.1·(32-1)	
3.1	3.1	4.4	2.2	1.8	0.9	-0.1·(-112)		4.4	3.1	3.9	-1.3	-2.6	2.2	-0.1·(-2-13)	
3.1	3.9	4.4	2.6	2.2	1.3	-0.1·(132)		4.4	3.9	3.1	-1.3	-2.2	2.6	-0.1·(23-1)	
3.1	3.1	4.4	1.8	2.2	0.9	-0.1·(-11-2)		4.4	3.1	3.1	-0.9	-1.8	2.2	-0.1·(211)	
3.9	3.1	4.4	2.2	2.6	1.3	-0.1·(312)		4.4	3.1	3.1	-0.9	-2.2	1.8	-0.1·(2-1-1)	
3.1	4.4	3.9	2.6	1.3	2.2	-0.1·(123)		3.1	3.9	4.4	2.6	-2.2	-1.3	-0.1·(-132)	
3.1	4.4	3.1	2.2	0.9	1.8	-0.1·(1-2-1)		3.1	3.1	4.4	1.8	-2.2	-0.9	-0.1·(11-2)	
3.1	4.4	3.1	1.8	0.9	2.2	-0.1·(12-1)		3.1	3.1	4.4	2.2	-1.8	-0.9	-0.1·(112)	
3.9	4.4	3.1	2.2	1.3	2.6	-0.1·(321)		3.9	3.1	4.4	2.2	-2.6	-1.3	-0.1·(3-1-2)	
4.4	3.1	3.9	1.3	2.6	2.2	-0.1·(213)		3.1	4.4	3.1	1.8	-0.9	-2.2	-0.1·(-12-1)	
4.4	3.1	3.1	0.9	2.2	1.8	-0.1·(2-11)		3.1	4.4	3.9	2.6	-1.3	-2.2	-0.1·(-123)	
4.4	3.1	3.1	0.9	1.8	2.2	-0.1·(-2-11)		3.1	4.4	3.1	2.2	-0.9	-1.8	-0.1·(121)	
4.4	3.9	3.1	1.3	2.2	2.6	-0.1·(231)		3.9	4.4	3.1	2.2	-1.3	-2.6	-0.1·(3-2-1)	
3.1	3.1	4.4	-2	-2	0.9	-0.1·(-112)		4.4	3.1	3.9	-1.3	2.6	-2.2	-0.1·(2-13)	
3.1	3.9	4.4	-3	-2	1.3	-0.1·(13-2)		4.4	3.9	3.1	-1.3	2.2	-2.6	-0.1·(-23-1)	
3.1	3.1	4.4	-2	-2	0.9	-0.1·(-112)		4.4	3.1	3.1	-0.9	1.8	-2.2	-0.1·(-211)	
3.9	3.1	4.4	-2	-3	1.3	-0.1·(31-2)		4.4	3.1	3.1	-0.9	2.2	-1.8	-0.1·(211)	

The illustration of hR lattice is represented by semi-reduced descriptions. The distance to the border hR - cI is -0.1, which corresponds to -0.123 given in $\Delta d/d$ units.

Table 5. Sixty-four semi-reduced descriptions of hR lattice ($a,b,c = 1.7607$; $\alpha,\beta,\gamma = 106.8773^\circ$) and its deformations to the cI lattice ($a,b,c = 2$; $\alpha,\beta,\gamma = 90^\circ$).

The last three lines give:

$$(4.4, 3.9, 3.1, -1.3, 2.2, -2.6) - 0.1·(-2-2, 3·3, -1·-1, -1·3, -1·-2, -2·3) = (4, 3, 3, -1, 2, -2)$$

$$(4.4, 3.1, 3.1, -0.9, 1.8, -2.2) - 0.1·(-2-2, 1·1, 1·1, 1·1, 1·-2, -2·1) = (4, 3, 3, -1, 2, -2)$$

$$(4.4, 3.1, 3.1, -0.9, 2.2, -1.8) - 0.1·(2·2, 1·1, 1·1, 1·1, 1·2, 2·1) = (4, 3, 3, -1, 2, -2)$$

The assigning of a symmetry group to a modified metric or comparing it with **Table 1** reveals *cI* symmetry in cI_{16} description. As a result, the distance from *hR* lattice ($a,b,c = 1.760682$; $\alpha,\beta,\gamma = 106.8773^\circ$) to *cI* lattice ($a,b,c = 2$; $\alpha,\beta,\gamma = 90^\circ$) is equal to -0.1 ($\Delta d/d = -0.123$) and as expected does not depend on the selected description. Theoretical descriptions of other *hR* lattices may be easily obtained: for example, by lowering ε 10 times $(4, 3, 3, -1, 2, -2) + 0.01 \cdot (2 \cdot 2, 1 \cdot 1, 1 \cdot 1, 1 \cdot 1, 1 \cdot 2, 2 \cdot 1) = (4.04, 3.01, 3.01, -0.99, 2.02, -1.98)$, which corresponds to the Bravais description: ($a,b,c = 1.734935$; $\alpha,\beta,\gamma = 109.2022^\circ$), $\varepsilon = -0.01$ and $\Delta d/d = -0.01467$.

The presence of random errors complicates the derivation of ε and $\Delta d/d$. If G approximately describes *hR* lattice, the distances to the borders will be also approximate. Assuming that $G = (4.41, 3.08, 3.12, -0.98, 2.23, -1.9)$ a threefold pseudo-symmetry axis can be found parallel to the [110] direction, which is nearly orthogonal to (211) planes. Least squares “best solution” of following equation

$$(4.41, 3.08, 3.12, -0.98, 2.23, -1.9) + \varepsilon \cdot (2 \cdot 2, 1 \cdot 1, 1 \cdot 1, 1 \cdot 1, 1 \cdot 2, 2 \cdot 1) = (4, 3, 3, -1, 2, -2)$$

gives $\varepsilon = -0.093$, which can be considered as a rather interesting result.

5.3. *hR-cP* border

To all cells contained in **Tables 4, 5** exact *hR* and approximate *cF* or *cI* symmetries are easily assigned by filtering V set only. No additional process of cell manipulation is necessary. But it is not true near *hR* – *cP* border: the exact *hR* symmetry can be recognized, but pseudo *cP* symmetry generally not. This discontinuity on the *hR* – *cP* border is caused by the fact that there is a unique semi-reduced description of *cP* lattice, namely, cP_0 (metric = 1,1,1,0,0,0). Any additional description of this lattice is not semi-reduced and its symmetry group contains symmetry matrices outside the considered V set. We are interested in finding such descriptions, which contain at least one *hR* subgroup in V . The problem, attacked from the *cF* and *cI* sides, leads to results included in **Table 6**.

Symbol	<i>cP</i> metric						Symbol	<i>cP</i> metric					
cP_1	1	1	2	-1	0	0	cP_{49}	1	1	2	-1	0	0
cP_2	1	1	2	0	-1	0	cP_{50}	1	1	2	0	-1	0
cP_3	1	1	2	0	1	0	cP_{51}	1	1	2	0	1	0
cP_4	1	1	2	1	0	0	cP_{52}	1	1	2	1	0	0
cP_5	1	2	1	-1	0	0	cP_{53}	1	2	1	-1	0	0
cP_6	1	2	1	1	0	0	cP_{54}	1	2	1	0	0	-1
cP_7	1	2	1	0	0	-1	cP_{55}	1	2	1	0	0	1
cP_8	1	2	1	0	0	1	cP_{56}	1	2	1	1	0	0
cP_9	2	1	1	0	1	0	cP_{57}	2	1	1	0	-1	0
cP_{10}	2	1	1	0	0	1	cP_{58}	2	1	1	0	0	-1
cP_{11}	2	1	1	0	0	-1	cP_{59}	2	1	1	0	0	1
cP_{12}	2	1	1	0	-1	0	cP_{60}	2	1	1	0	1	0
cP_{13}	1	2	2	1	1	1	cP_{61}	1	1	3	-1	-1	0
cP_{14}	1	2	2	-1	-1	1	cP_{62}	1	1	3	-1	1	0
cP_{15}	1	2	2	-1	1	-1	cP_{63}	1	1	3	1	-1	0

Symbol	cP metric						Symbol	cP metric					
cP_{16}	1	2	2	1	-1	-1	cP_{64}	1	1	3	1	1	0
cP_{17}	1	2	2	-1	-1	0	cP_{65}	1	3	1	-1	0	-1
cP_{18}	1	2	2	-1	0	-1	cP_{66}	1	3	1	-1	0	1
cP_{19}	1	2	2	1	1	0	cP_{67}	1	3	1	1	0	-1
cP_{20}	1	2	2	1	0	1	cP_{68}	1	3	1	1	0	1
cP_{21}	1	2	2	1	-1	0	cP_{69}	3	1	1	0	-1	-1
cP_{22}	1	2	2	1	0	-1	cP_{70}	3	1	1	0	-1	1
cP_{23}	1	2	2	-1	1	0	cP_{71}	3	1	1	0	1	-1
cP_{24}	1	2	2	-1	0	1	cP_{72}	3	1	1	0	1	1
cP_{25}	2	1	2	1	1	1	cP_{73}	2	1	3	-1	-2	1
cP_{26}	2	1	2	-1	-1	1	cP_{74}	2	1	3	-1	2	-1
cP_{27}	2	1	2	-1	1	-1	cP_{75}	2	1	3	1	-2	-1
cP_{28}	2	1	2	1	-1	-1	cP_{76}	2	1	3	1	2	1
cP_{29}	2	1	2	-1	-1	0	cP_{77}	2	3	1	-1	-1	2
cP_{30}	2	1	2	0	-1	-1	cP_{78}	2	3	1	-1	1	-2
cP_{31}	2	1	2	1	1	0	cP_{79}	2	3	1	1	-1	-2
cP_{32}	2	1	2	0	1	1	cP_{80}	2	3	1	1	1	2
cP_{33}	2	1	2	1	-1	0	cP_{81}	3	1	2	-1	-2	1
cP_{34}	2	1	2	0	1	-1	cP_{82}	3	1	2	-1	2	-1
cP_{35}	2	1	2	-1	1	0	cP_{83}	3	1	2	1	-2	-1
cP_{36}	2	1	2	0	-1	1	cP_{84}	3	1	2	1	2	1
cP_{37}	2	2	1	1	1	1	cP_{85}	1	2	3	-2	-1	1
cP_{38}	2	2	1	-1	-1	1	cP_{86}	1	2	3	-2	1	-1
cP_{39}	2	2	1	-1	1	-1	cP_{87}	1	2	3	2	-1	-1
cP_{40}	2	2	1	1	-1	-1	cP_{88}	1	2	3	2	1	1
cP_{41}	2	2	1	-1	0	-1	cP_{89}	1	3	2	-2	-1	1
cP_{42}	2	2	1	0	-1	-1	cP_{90}	1	3	2	2	-1	-1
cP_{43}	2	2	1	1	0	1	cP_{91}	1	3	2	2	1	1
cP_{44}	2	2	1	0	1	1	cP_{92}	1	3	2	-2	1	-1
cP_{45}	2	2	1	1	0	-1	cP_{93}	3	2	1	-1	-1	2
cP_{46}	2	2	1	0	1	-1	cP_{94}	3	2	1	-1	1	-2
cP_{47}	2	2	1	-1	0	1	cP_{95}	3	2	1	1	-1	-2
cP_{48}	2	2	1	0	0	1	cP_{96}	3	2	1	1	1	2

Small rhombohedral deformations change descriptions in the table into semi-reduced forms of hR lattices. Positive deformations allow to continuously transform cP into cF ($cP_1 - cP_{48} \rightarrow cF_1 - cF_{16}$). Similarly, negative deformations transform cP into cI ($cP_{49} - cP_{96} \rightarrow cI_1 - cI_{16}$). Twelve metrics ($cP_1 - cP_{12}$ and $cP_{49} - cP_{60}$) coincide. The cP0 case links all primitive and centered cubic lattices by rhombohedral deformations.

Table 6. Non-semi-reduced descriptions of cP lattices close to semi-reduced hR.

For all *cP* descriptions in **Table 6**, the filtering of V fails in obtaining a complete set of symmetry matrices and assigning *cP* Bravais type, but in all cases the matrices comprise at least one complete *hR* group, indicated geometrically by symbols of threefold axes with corresponding directions and Miller indices. Rhombohedral deformations based on obtained (hkl) 's and assumed $\varepsilon > 0$ transform cP_1 - cP_{48} into 60 semi-reduced variants of some *hR* lattice. Together with 4 variants arising from cP_0 (1,1,1,0,0,0), the total number is again 64. All are equi-distanted from the *cP* lattice. Similar analysis leads to 64 semi-reduced *hR* descriptions obtained from cP_{49} - cP_{96} and cP_0 by rhombohedral distortion with $\varepsilon < 0$.

In the neighborhood of cubic symmetry, the semi-reduced *hR* lattices reveal distorted rhombohedral *cF*, *cI*, or *cP* pseudo-symmetries and exact *hR* symmetry. The distortion can be extracted from the lattice metric using the geometric information from the 'strict' threefold axis. The distance to the border given by ε or $\Delta d/d$ value does not depend on the lattice description (64 semi-reduced variants). Such distance corresponds to the angular differences: α -60°, α -90°, α -109.47° for a conventional description of *hR* lattice.

6. Distances between *hR* and monoclinic lattices: composed deformations

As mentioned earlier, the symmetry axis splits orthogonally 3D lattice into union of 1D lattice and 2D lattice and is stable during uniaxial deformation in 1D direction. But a twofold axis is less restrictive in comparison with higher order axes, and in this case 2D lattice can also be modified. This complicates the modeling of *mC*-*hR* border and the calculation of distance from *mC* to *hR* lattices. The modeling is simplified if the *hR* lattice description is restricted to the conventional form ($a = b = c$, $\alpha = \beta = \gamma < 120^\circ$). The geometric interpretation of symmetry is characterized by dual symbols: 3+111, 3-111, 201-1, 21-10, 2-101. The dot product $[uvw] \cdot (hkl)$ is 2 for all twofold axes, which means that deformation $\varepsilon(hkl)$, where $(hkl) = (01-1)$, $(1-10)$, (-101) , transforms an *hR* lattice to the centered monoclinic, for example, *mC*. Other ε deformations are also possible. For a twofold axis in $[uvw]$ direction, any deformation $\varepsilon(hkl)$, where $[uvw] \cdot (hkl) = 0$, retains the given twofold symmetry. Moreover, small deformations are additive and their (hkl) -type can be recognized by geometric images (**Table 7**).

$\Delta a/a [\%]$	$\Delta b/b [\%]$	$\Delta c/c [\%]$	$\Delta\alpha [^\circ]$	$\Delta\beta [^\circ]$	$\Delta\gamma [^\circ]$	$\delta [^\circ]$	Operation
Deformation 0.001·(01-1) → <i>mC</i> (1, 1.0320, 1.7143, 90°, 123.2094°, 90°)							
0.0000	0.0000	0.0000	0.0000	0.0000	0.0000	0.0000	201-1
0.0500	-0.0500	0.0000	-0.0800	0.0800	0.0000	0.0934	21-10
0.0500	0.0000	-0.0500	-0.0800	0.0000	0.0800	0.0934	2-101
0.0500	0.0000	-0.0500	-0.0800	0.0000	0.0800	0.0000	3+111
0.0500	-0.0500	0.0000	-0.0800	0.0800	0.0000	0.0000	3-111
Deformation 0.001·(011) → <i>mC</i> (1, 1.0301, 1.7155, 90°, 123.1840°, 90°)							
0.0000	0.0000	0.0000	0.0000	0.0000	0.0000	0.0000	201-1
0.0500	-0.0500	0.0000	0.0496	-0.0496	0.0000	0.0556	21-10

$\Delta a/a [\%]$	$\Delta b/b [\%]$	$\Delta c/c [\%]$	$\Delta\alpha [^\circ]$	$\Delta\beta [^\circ]$	$\Delta\gamma [^\circ]$	$\delta [^\circ]$	Operation
0.0500	0.0000	-0.0500	0.0496	0.0000	-0.0496	0.0556	2-101
0.0500	0.0000	-0.0500	0.0496	0.0000	-0.0496	0.0532	3+111
0.0500	-0.0500	0.0000	0.0496	-0.0496	0.0000	0.0532	3-111
Deformation $0.001 \cdot (01-1) + 0.001 \cdot (011) \rightarrow mC (1, 1.0320, 1.7155, 90^\circ, 123.1840^\circ, 90^\circ)$							
0.0000	0.0000	0.0000	0.0000	0.0000	0.0000	0.0000	201-1
0.1000	-0.0999	0.0000	-0.0304	0.0304	0.0000	0.0774	21-10
0.1000	0.0000	-0.0999	-0.0304	0.0000	0.0304	0.0774	2-101
0.1000	0.0000	-0.0999	-0.0304	0.0000	0.0304	0.0532	3+111
0.1000	-0.0999	0.0000	-0.0304	0.0304	0.0000	0.0532	3-111

Geometric images of monoclinic simple deformations $0.001 \cdot (01-1)$, $0.001 \cdot (011)$ and composed deformation $0.001 \cdot (01-1) + 0.001 \cdot (011) = 0.002 \cdot (010)$. Resulting monoclinic lattice parameters are given explicitly.

Table 7. Examples of the border $hR-mC$ models for hR lattice ($a,b,c = 1$, $\alpha,\beta,\gamma = 62^\circ$).

The ε -deformations are additive by the definition, but this feature is also valid for geometric images (excluding δ) in the vicinity of a border, as was exemplified in **Table 7**. This feature means that more complicated images can be decomposed and explained by a few ε -deformations, at least in theory. In this situation, the goal is to obtain $maxdev \approx 0$ by uniaxial deformations of a probe cell, where deformation types (hkl)'s can be predicted from the geometric images. The introductory application of such analysis is shown in the following two real-life examples.

7. The distances for phospholipase A₂

For a comparative study of different distances between a probe cell and the items in protein database (PDB), McGill and others [2] used unit cells of phospholipase A₂ discussed in [12], which concluded that items 1g2x, 1u4j, and 1fe5 describe the same structure. Study, among other interesting conclusions, showed a similarity only between 1g2x and 1u4j cells for all applied distances. This result is also confirmed by analysis based on ε distances (**Table 8**).

1g2x	80.949	80.572	57.098	90°	90.35°	90°	C
1u4j	80.36	80.36	99.44	90°	90°	120°	R
1fe5	57.98	57.98	57.98	92.02°	92.02°	92.02°	P
1g2x	3260.18	3261.15	3261.15	15.22	14.12	14.12	original
$\varepsilon = -1.04 \cdot (011) + 0.07 \cdot (01-1)$				deformation: monoclinic			
3260.18	3260.18	3260.18	3260.18	14.12	14.12	14.12	hR
$\varepsilon = -14.12 \cdot (111)$				deformation: rhombohedral			
3246.06	3246.06	3246.06	3246.06	0.00	0.00	0.00	cP

1u4j	3251.28	3251.28	3251.28	22.41	22.41	22.41	original
	$\varepsilon = -22.41 \cdot (111)$			deformation: rhombohedral			
	3228.87	3228.87	3228.87	0.00	0.00	0.00	cP
1fe5	3361.68	3361.68	3361.68	-118.49	-118.49	-118.49	original
	$\varepsilon = 118.49 \cdot (111)$			deformation: rhombohedral			
	3480.17	3480.17	3480.17	0.00	0.00	0.00	cP

Upper lines give standard Bravais descriptions for three items. Corresponding three parts compare original metric tensors, ε distances to higher symmetry borders, and metric tensors of these borders for each item.

Table 8. Original cell data for PDB items (1g2x, 1u4j, 1fe5) and ε distances to higher symmetry borders.

The monoclinic deformation of 1g2x cell is very small. Rhombohedral distances ε to the cubic border are similar for 1g2x and 1u4j, but drastically different in comparison with that in 1fe5. Moreover, the different sign suggests that if one agrees that all three items describe the same structure it must also allow the possibility that the true symmetry is cubic. It is also visible that this method is sensitive for much smaller (then analyzed) deviations from the symmetry borders.

8. *hR-mC* dilemma in $\alpha\text{-Cr}_2\text{O}_3$, $\alpha\text{-Fe}_2\text{O}_3$, CaCO_3

The crystal structures of BiFeO_3 , as well as of $\alpha\text{-Cr}_2\text{O}_3$, $\alpha\text{-Fe}_2\text{O}_3$, CaCO_3 are usually described as trigonal, but there are motivations that come from systematic (*hkl*) peak broadening and anisotropic microstrains, indicating monoclinic deformations, to assume that an average metric structure reveals monoclinic, that is, broken symmetry. [3, 4] Such broadening is systematic and increases with the crushing polycrystalline powders in a planetary mill and thus, at least in theory, can modify symmetry. High-resolution synchrotron radiation powder diffractions and Rietveld refinement were used in [3, 4] to obtain precise cell parameters. Values of agreement factors obtained with the Rietveld refinement of the trigonal and monoclinic models were very similar. The authors concluded that the lowering of symmetry should result in splitting some diffraction lines, which was not observed.

Let us look at the published data obtained for the monoclinic model [3, 4]. Cell parameters were recalculated to the primitive form, which was not Niggli. The strict symmetry had geometric description 2 1–10. Therefore, it was assumed that composite deformation $\varepsilon_1(1-10) + \varepsilon_2(110)$ brings these monoclinic cells to the rhombohedral ones. The BiFeO_3 cell data were not available but all the data for $\alpha\text{-Cr}_2\text{O}_3$, $\alpha\text{-Fe}_2\text{O}_3$, CaCO_3 and different milling times reveal similar values $\varepsilon_1 = \varepsilon_2 \approx -0.004$. Values do not depend on the milling time, even if systematically broadened peaks are shown. Deviations from *hR* borders in the form of $\Delta d/d \approx -0.0004$ mean that it is practically not possible to observe the line splitting. A strict and systematic relationship $\varepsilon_1 = \varepsilon_2$ seems to be nonphysical, rather a result of the monoclinic constrains in Rietveld refinements. Despite the high precision of synchrotron powder diffraction, a monoclinic lattice deformation was not metrically determined.

9. Summary

Generally, border problems cannot be overlooked in s.r.d. Small, but not negligible, values of discrepancy parameters indicate the border problem and give some measure to the higher symmetry border. Deviations in isometric actions on the investigated cell can be explained by monoaxial deformations measured by parameter ε or by $\Delta d/d$, which is more informative for powder diffraction investigations.

Moreover, ε is not dependent on the choice of lattice representation in s.r.d. It was explicitly shown in **Tables 4** and **5**. These data can be also used for testing other definitions of distances, because 64 items describe the same rhombohedral lattice (distances between items should be zero and between each item and the cubic cF and cI lattices should be fixed). The situation is more complicated in the vicinity of cP border. Pseudo- cP symmetry cannot be recognized for most s.r.d. representations of hR lattices, since they are similar to non-semi-reduced cP descriptions listed in **Table 6**. But there is still a possibility to select such hR description, which is simultaneously Niggli-reduced, and to find the distance to cP_0 .

The concept is outlined and tested for hR lattices, but for wider applications other lattice types (especially cubic) should be investigated.

Author details

Kazimierz Stróż

Address all correspondence to: kazimierz.stroz@us.edu.pl

Faculty of Computer Science and Material Sciences, University of Silesia, Katowice, Poland

References

- [1] Maciček J, Yordanov A. BLAF – A robust program for tracking out admissible Bravais lattice(s) from the experimental unit-cell data. *Journal of Applied Crystallography*. 1992;**25**:73-80
- [2] McGill KJ, Asadi M, Karkasheva MT, Andrews LC, Bernstein HJ. The geometry of Niggli reduction: SAUC – Search of alternative unit cells. *Journal of Applied Crystallography*. 2014;**47**:360-364
- [3] Stękiel M, Przeniosło R, Sosnowska I, Fitch A, Jasiński JB, Lussier JA, Bieringer M. Lack of a threefold rotation axis in α -Fe₂O₃ and α -Cr₂O₃ crystals. *Acta Crystallographica*. 2015;**B71**:203-208
- [4] Przeniosło R, Fabrykiewicz P, Sosnowska I. Monoclinic deformation of calcite crystals at ambient conditions. *Physica B*. 2016;**496**:49-56

- [5] Himes VL, Mighell AD. A matrix method for lattice symmetry determination. *Acta Crystallographica*. 1982;**A38**:748-749
- [6] Himes VL, Mighell AD. A matrix approach to symmetry. *Acta Crystallographica*. 1987;**A43**:375-384
- [7] Le Page Y. The derivation of the axes of the conventional unit cell from the dimensions of the Buerger-reduced cell. *Journal of Applied Crystallography*. 1982;**15**:255-259
- [8] Stróż K. Space of symmetry matrices with elements 0, ± 1 and complete geometric description; its properties and application. *Acta Crystallographica*. 2011;**A67**:421-429
- [9] Stróż K. Symmetry of semi-reduced lattices. *Acta Crystallographica*. 2015;**A71**:268-278
- [10] Stróż K. A systematic approach to the derivation of standard orientation-location parts of symmetry-operation symbols. *Acta Crystallographica*. 2007;**A63**:447-454
- [11] Andrews CL, Bernstein HJ. The geometry of Niggli reduction: BGAOL – Embedding Niggli reduction and analysis of boundaries. *Journal of Applied Crystallography*. 2014;**47**:346-359
- [12] Le Trong I, Stenkamp RE. An alternate description of two crystal structures of phospholipase A₂ from *Bungarus caeruleus*. *Acta Crystallographica*. 2007;**D63**:548-549